Thrombin Impairs Alveolar Fluid Clearance by Promoting Endocytosis of Na^+,K^+-ATPase

István Vadász, Rory E. Morty, Andrea Olschewski, Melanie Königshoff, Markus G. Kohstall, Hossein A. Ghofrani, Friedrich Grimminger, and Werner Seeger

University of Giessen Lung Center, Justus-Liebig-University Giessen, Giessen, Germany

Coagulation is an emerging area of interest in the pathogenesis and treatment of acute lung injury. Concentrations of the edemagenic coagulation protease thrombin are elevated in plasma and lavage fluids from afflicted patients. We explored the impact of thrombin on the formation and resolution of alveolar edema. Intravascularly applied thrombin inhibited active transepithelial ^{22}Na transport in intact rabbit lungs, suppressing alveolar fluid clearance. Epithelial permeability was unaffected, whereas endothelial permeability was increased. In A549 human lung epithelial cells and in mouse primary alveolar type II cells, thrombin blocked ouabain-sensitive Na^+,K^+-ATPase-mediated $^{86}Rb^+$ uptake, without altering amiloride-sensitive sodium currents. Furthermore, thrombin downregulated cell-surface expression of Na^+,K^+-ATPase, but not ENaC α and β subunits. The endocytosis inhibitor phalloidin oleate blocked all thrombin-induced effects on sodium transport activity. Similarly, diphenyleneiodonium chloride, an inhibitor of reactive oxygen radical production, as well as a protein kinase C-ζ inhibitor, prevented these thrombin-induced effects. Thus, thrombin signaling via reactive oxygen species and protein kinase C-ζ promotes Na^+,K^+-ATPase endocytosis, resulting in loss of function. We propose here a dual role for thrombin in mediating disturbances to fluid balance in the lung: thrombin concomitantly provokes edema formation by increasing endothelial permeability, and inhibits alveolar edema resolution by blocking Na^+,K^+-ATPase function.

Keywords: acute respiratory distress syndrome; coagulation; permeability; protein kinase C-ζ; reactive oxygen species

Acute lung injury/acute respiratory distress syndrome (ALI/ARDS) is an important cause of morbidity and mortality in critically ill patients, with an incidence of up to 75 per 100,000 (1), and exhibiting mortality rates of between 31 and 74% (2). One of the hallmarks of ALI/ARDS is the influx of protein-rich edema fluid into the alveolar space (1). This occurs as a result of increased permeability of the alveolar–capillary barrier, which itself is formed by two separate barriers, the microvascular endothelium and the alveolar epithelium (3). Damage to both the endothelial (1) and the epithelial (4) barriers promotes alveolar flooding, and loss of epithelial barrier integrity impairs alveolar fluid clearance (5). It has been well established that the ability of the ALI/ARDS patient to clear alveolar edema fluid is associated with a shorter stay in the intensive care unit, and with reduced mortality (6, 7).

(*Received in original form December 20, 2004 and in final form July 9, 2005*)

Supported by the Deutsche Forschungsgemeinschaft Schwerpunktprogramm 1028 and Sonderforschungsbereich 547 "Kardiopulmonales Gefäßsystem." I.V. is supported by a predoctoral fellowship from ALTANA Pharma. R.E.M. is a Fellow of the Alexander von Humboldt Foundation.

Correspondence and requests for reprints should be addressed to Werner Seeger, M.D., University of Giessen Lung Center, Medical Clinic II, Justus Liebig University, Klinikstrasse 36, D-35392 Giessen, Germany. E-mail: Werner.Seeger@innere.med.uni-giessen.de

Am J Respir Cell Mol Biol Vol 33. pp 343–354, 2005
Originally Published in Press as DOI: 10.1165/rcmb.2004-0407OC on July 13, 2005
Internet address: www.atsjournals.org

Coagulation proteases such as thrombin have been accredited with a key role in the pathogenesis of ALI/ARDS (8). Procoagulant activity attributable to tissue factor–factor VIIa is dramatically elevated in the bronchoalveolar lavage (BAL) fluids (9, 10) and plasma (11) of patients with ALI/ARDS, which may result in the activation of prothrombin to thrombin. Clinical studies have documented an increase in prothrombin activation fragment F1+2 and thrombin–antithrombin III complexes, two markers of thrombin generation, in patients with ALI progressing to ARDS (12).

Proposed roles for coagulation proteases in ALI/ARDS include the generation of microvascular fibrin deposition products (13) and disseminated intravascular coagulation (14), which mediate inflammatory reactions in the lung (15). Thus, anticoagulants are emerging as new and exciting therapeutic agents for the treatment of ARDS (16), and coagulation proteases are currently the subject of intense study with respect to a role in ARDS pathogenesis (17).

Thrombin can directly influence epithelial and endothelial barrier integrity *in vitro* (18). In endothelial cell monolayers, thrombin directly increases endothelial permeability to albumin (19) by direct activation of thrombin receptors, which in turn activate multiple signaling pathways involving Rho kinase (20) and myosin light chain kinase (21). The effect of thrombin on epithelial barrier integrity is less well studied; however, one study suggests that thrombin can directly decrease the permeability of epithelial cell monolayers of human bronchial epithelial cells, and the A549 human lung epithelial cell line (18). In contrast, in a live animal model, thrombin increased lung epithelial permeability, and this permeability increase was dependent on the activation of intravascular coagulation (22).

These thrombin-induced changes in the endothelial, and perhaps epithelial barrier have led several investigators to propose a role for thrombin (and other coagulation factors) as an edemagenic factor in the lung, promoting interstitial and/or alveolar flooding. Indeed, intravascular application of thrombin provokes edema in an isolated guinea pig lung (23). However, no studies to date have addressed a potential role for the coagulation proteases in the resolution of pulmonary edema. In this study, we demonstrate that thrombin can indeed impair alveolar fluid clearance. As such, this study adds to the growing body of data implicating this important protease as an integral pathogenic factor in ALI/ARDS.

Some of the results of these studies have been previously reported in the form of a poster discussion presented at the 2005 International Conference of the American Thoracic Society, San Diego, California, May 20–25, 2005 (24).

MATERIALS AND METHODS

Lung Preparation and Handling

Lungs were isolated from healthy adult male rabbits (Charles River, Sulzfeld, Germany) weighing 3.0 ± 0.5 kg, as described previously (25, 26). Lungs were perfused by re-circulation of Krebs-Henseleit buffer (120 mM NaCl, 4.3 mM KCl, 1.1 mM KH_2PO_4, 25 mM $NaHCO_3$, 2.4 mM $CaCl_2$, 1.3 mM magnesium phosphate, 0.24% [m/vol] glucose and

5% [m/vol] hydroxyethylamylopectin) at a flow-rate of 100 ml/min with a left atrial pressure of 1.6 mm Hg, via catheters inserted into the pulmonary artery and the left atrium exactly as previously described (25). Lungs were ventilated with room air supplemented with 4.5% CO_2 to maintain pH of the recirculating buffer between 7.35 and 7.37. Peak inspiratory pressure was set to 7.5 mm Hg. A frequency of 30 breaths/min and an inspiratory/expiratory ratio of 1:1 with a positive end-expiratory pressure (PEEP) of 2 mm Hg was applied to prevent atelectasis and to maintain constant minute volume during the experiment. Perfusion pressure, ventilation pressure, and the weight of the isolated organ were continuously monitored online.

Treatment of Lungs

Lungs were allowed to establish steady-state baseline conditions for 30 min, after which lungs were either nebulized with physiologic saline (in the case of sham nebulization) or with amiloride or phalloidin oleate in 2.5% (vol/vol) dimethyl sulfoxide (DMSO) in physiologic saline, yielding a concentration of 10 μM amiloride or 1 μM phalloidin oleate in the epithelial lining fluid (ELF). This first nebulization (duration 5 min) deposited 0.5 ml of fluid into the alveolar space, with a concomitant 0.5 g transient increase in lung weight, attributable to this fluid that was nebulized into the lung (Figure 1, *dashed boxes*). Lungs were allowed to reestablish steady-state baseline conditions for 30 min, after which thrombin (2.5 U/ml) was applied to the perfusate. In some experiments, phalloidin oleate and then thrombin were applied sequentially in the same experiment, as described above. Experiments were conducted either at 37°C or at 4°C. After a 30-min re-equilibration period, radioactive tracers were applied by ultrasonic nebulization of a mixture of ^{22}NaCl (1 μCi/ml) and [^{3}H]mannitol (6 μCi/ml) in physiologic saline, over 10 min, with an Optineb ultrasonic nebulizer (Nebu-Tec, Elsenfeld, Germany), connected directly to the inspiration loop of the ventilator, leading to a tracer deposition of ~1 μCi $^{22}Na^+$, and ~6 μCi [^{3}H]mannitol (25). This second nebulization deposited 1 ml of fluid into the alveolar space, with a concomitant 1-g increase in lung weight, attributable to this fluid that was nebulized into the lung (Figure 1, *solid boxes*). Kinetics of $^{22}Na^+$ and [^{3}H]mannitol tracer clearance were determined exactly as described previously (25). These experimental protocols are illustrated in Figure 1. Immediately after the termination of perfusion, the bronchoalveolar space was lavaged with 30 ml of unlabeled isoosmolar mannitol. The entire volume was bolus injected into the trachea and immediately reaspirated gently. The original 30-ml lavage was reinjected into the trachea, and reaspirated two times (i.e., a total of three injection–aspiration cycles were performed with the same 30 ml lavage fluid). The total lavage time did not exceed 15 s. The mixed BAL fluid that was reaspirated out of the lungs (recovery 75–80% in all experiments) was then centrifuged at 300 × *g* for 10 min to separate the cells from the supernatant. The sodium concentrations in the perfusate and BAL fluid were assessed with a highly sensitive ion-selective electrode (Mettler Toledo, Giessen, Germany). This electrode possesses linearity for sodium in the range from 1×10^{-5} to 1×10^{3} mM, with < 0.1% cross-sensitivity for other ions. Assuming that the concentration of sodium in the epithelial lining layer corresponds to that in the vascular fluid (in this case, perfusion medium) (27) in the absence of sodium in the instillation fluid, the relationship between volume and sodium concentration in the mixed BAL fluid and the ELF can be expressed by $(V_{BAL} + V_{ELF}) \times [Na]_{BAL(mixed)} = V_{ELF} \times [Na]_{ELF}$, where V_{BAL} is the volume of the instillate (in this case 30 ml), V_{ELF} is the volume of ELF, $[Na]_{BAL(mixed)}$ is the concentration of sodium in the mixed BAL fluid, and $[Na]_{ELF}$ is the concentration of sodium in the ELF (equal to the sodium concentration in the perfusate). Resolution of this equation yields $V_{ELF} = \{V_{BAL} \times [Na]_{BAL(mixed)}\}/\{[Na]_{ELF} - [Na]_{BAL(mixed)}\}$. The time-frame of our lavage (15 s) has been shown previously to be rapid enough to avoid significant additional sodium entry into the alveolar space during the lavage procedure itself (28). Furthermore, this time-frame is sufficient to allow adequate mixing of ELF with lavage fluid, since when we load fluid into the lung (by nebulization) the fluid volume that we load into the lung is accurately reflected by an increase in the calculated ELF volume, a value that is derived from the BAL fluid, as we have reported previously (26). The measured sodium concentrations and calculated ELF volumes are reported in Table 1.

Electrophysiology

To investigate thrombin- and amiloride-induced changes in macroscopic current, we employed the conventional whole-cell patch-clamp technique (29) essentially as described previously (25). A549 cells were obtained from the American Type Culture Collection (Manassas, VA) and primary murine alveolar epithelial type II (ATII) cells were isolated as described by Corti and colleagues (30) from C57/Bl6 mice. The ATII cell preparations were > 95% viable (as determined by trypan blue dye exclusion), and 92–96% pure (as determined by lamellar body staining with phosphine 3R or Nile Red). Briefly, cells were plated on coverslips and mounted in a flow-through chamber on the stage of an inverted microscope (Axiovert 135; Zeiss, Jena, Germany) and perfused (2–3 ml/min) with the bath solution using a gravity-driven perfusion system. Pipettes pulled from borosilicate glass tubes (GC 150; Clark Electromedical Instruments, Pangbourne, UK) were fire-polished to

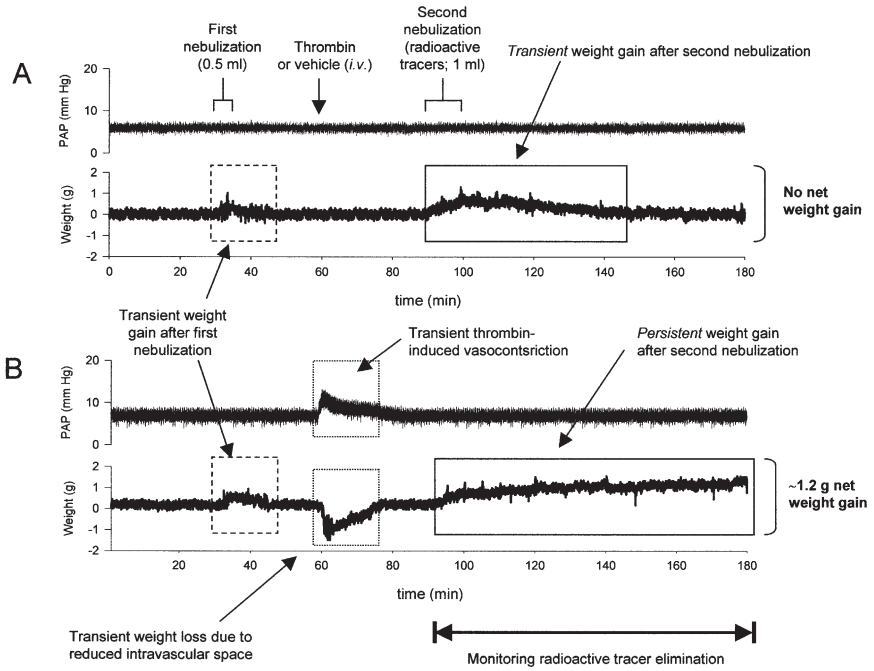

Figure 1. Thrombin prevents fluid reabsorption in an isolated, ventilated, and perfused rabbit lung model. Experimental protocol. Original representative recordings of pulmonary arterial pressure (PAP) and lung weight for a control lung (*A*) and a thrombin-treated lung (*B*) at 37°C are indicated. Transient postnebulization weight gains of the lungs after a 0.5-ml fluid challenge ("first nebulization"; either physiologic saline, in the case of a sham nebulization; or amiloride or phalloidin oleate) are indicated by the *dashed box*. A transient vasoconstriction after thrombin administration caused a transient increase in PAP, accompanied by a transient decrease in lung weight. These phenomena are indicated in the *dotted box*. The transient weight gain of control lungs after a second fluid challenge of 1 ml ("second nebulization") is indicated by a *solid box* in *A*. In addition to the postnebulization weight gain, there is a persistent increase of weight over the entire experiment in thrombin-treated lungs (*solid box* in *B*).

TABLE 1. EXPERIMENTALLY-DETERMINED SODIUM CONCENTRATIONS, CALCULATED EPITHELIAL LINING FLUID VOLUMES, AND WET-TO-DRY WEIGHT RATIOS FOR ISOLATED, VENTILATED, AND PERFUSED RABBIT LUNGS

			Termination of experiment (3 h)					
	Before lung isolation	After steady-state	Untreated	4°C	Thrombin (*2.5 U/ml*)	Amiloride (*10 μM*)	PO (*1 μM*)	Thrombin (*2.5 U/ml*)+PO (*1 μM*)
[Na^+] (mM) in mixed BAL fluid	3.24 ± 0.39	11.14 ± 1.33	11.36 ± 0.98	17.52 ± 1.09	14.85 ± 1.14	14.13 ± 0.48	11.74 ± 1.41	12.46 ± 1.13
V_{ELF} (ml)	0.66 ± 0.08	2.41 ± 0.31	2.46 ± 0.23	3.97 ± 0.28	3.3 ± 0.28	3.12 ± 0.12	2.55 ± 0.33	2.72 ± 0.27
W/D	5.57 ± 0.18	6.52 ± 0.26	6.49 ± 0.40	7.79 ± 0.42	7.20 ± 0.18	7.25 ± 0.32	6.53 ± 0.27	6.67 ± 0.34

Definition of abbreviations: BAL, bronchoalveolar lavage; PO, phalloidin oleate; VELF, epithelial lining fluid volumes; W/D, wet:dry weight ratios.

give a final resistance of 3–4 MΩ. The patch-clamp amplifier was an Axopatch 200B (Axon Instruments, Foster City, CA). The effective corner frequency of the low pass filter was 5 kHz. The frequency of digitization was twice that of the filter frequency. The data were stored and analyzed using commercially available software (pCLAMP; Axon Instruments). Offset potentials were nulled directly before formation of a seal. Experiments were performed at room temperature. The A549 cells were perfused with 145 mM NaCl, 2.7 mM KCl, 1.8 mM $CaCl_2$, 2 mM $MgCl_2$, 5.5 mM glucose, and 10 mM HEPES, pH 7.4 (bath-1). Pipettes were back-filled with 135 mM potassium methylsulfonic acid, 10 mM KCl, 6 mM NaCl, 1 mM Mg_2ATP, 2 mM Na_2ATP, 5.5 mM glucose, 10 mM HEPES, and 1 mM EGTA, pH 7.4 (pipette-1). Whole cell currents of ATII cells were recorded in essential symmetrical sodium isethionate solutions (bath-2 and pipette-2 solutions). Bath-2 solution contained 140 mM sodium isethionate, 5 mM K-isethionate, 10 mM HEPES, 1.2 mM $MgSO_4$, 1 mM $CaSO_4$, and 5 mM glucose, pH 7.4. Pipette-2 solution contained 140 mM sodium isethionate, 5 mM potassium isethionate, 10 mM HEPES, 1.2 mM $MgSO_4$, 1 mM EGTA, and 5 mM glucose, pH 7.2. Only those cells containing the granular inclusions typical of type II cell morphology were chosen for the study. Inward and outward currents across the cell membrane were elicited by employing a step-pulse protocol from −100 to +100 mV in 10-mV (A549 cells) or 20-mV (ATII cells) increments for a duration of 500 ms (A549 cells) or 50 ms (ATII cells) from a holding potential of −40 mV (A549 cells) or 0 mV (ATII cells). Current–voltage (I–V) relationships were constructed by averaging the current values between 100 and 500 ms (A549 cells) or 10 and 50 ms (ATII cells) from the start and plotted using Origin Software (Microcal Software, Northampton, MA). The drug-sensitive currents were calculated by subtracting the current remaining after exposure to thrombin or thrombin and amiloride from the corresponding control (no drug) values in A549 cells (25, 31, 32).

Ouabain-Sensitive Rubidium-Uptake Assay

Ouabain-sensitive uptake of the K^+-mimic $^{86}Rb^+$ into A549 and ATII cells was used to estimate potassium transport mediated by Na^+,K^+-ATPase, essentially as described previously (25) with the following modifications. Cells were maintained in Dulbecco's modified Eagle's medium (DMEM) supplemented with 10% (vol/vol) fetal bovine serum. However, 1 h before use, cells were washed with phosphate-buffered saline (PBS) (3×) and the medium was replaced with serum-free DMEM. In some cases, cells were preincubated with phalloidin oleate, a cell-permeable phalloidin analog that inhibits endocytosis (1 μM; Sigma, St. Louis, MO) for 30 min before addition of thrombin (10 – 0.05 U/ml). Ouabain was employed at 5 mM to determine ouabain-sensitive activity. The generation of ROS was blocked by 15 min preincubation with diphenyleneiodonium chloride (DPI; 5 μM) or rotenone (1 μM) before the addition of thrombin (10 U/ml). The DPI was freshly prepared and used immediately, under conditions which have previously been reported by our laboratory to yield maximum inhibition of ROS generation (33, 34). Protein kinase C (PKC)-dependent signaling pathways were blocked by 15 min preincubation with a cell-permeable myristoylated general pseudosubstrate peptide antagonist of PKC (myr-RFARKGALRQKNV; 40 μM), or a cell-permeable myristoylated specific pseudosubstrate peptide antagonist of PKC-ζ (myr-SIYRRGARRWRKL; 15 μM) before the addition of thrombin (10 U/ml).

Cell-Surface Biotinylation of Na^+,K^+-ATPase and ENaC

Biotinylation of cell-surface proteins of A549 and ATII cells was undertaken as described previously (35) as modified in (25). Cells were treated exactly as described above for "ouabain-sensitive rubidium-uptake assay", and cell extracts were prepared in 50 mM Tris-Cl, 150 mM NaCl, 1% (vol/vol) NP-40, and 1% (m/vol) sodium deoxycholate, pH 8, supplemented with Complete protease inhibitor cocktail (Roche, Mannheim, Germany). For biotinylation studies, equal amounts of protein (usually 150 μg) were employed for each condition, and were incubated with streptavidin-agarose beads. After biotinylation, the Na^+,K^+-ATPase was detected with mouse monoclonal $IgG_{1\kappa}$ anti-Na^+,K^+-ATPase α-1 subunit (clone C464.6; Upstate, Waltham, MA), while ENaC was detected with mouse monoclonal $IgG_{1\kappa}$ anti-ENaC β subunit (clone B-3) or goat polyclonal IgG anti-ENaC α subunit (Calbiochem, San Diego, CA).

Assessment of Endothelial Permeability

Capillary filtration coefficients ($K_{f,c}$) were measured to assess changes in endothelial permeability. Coefficients were determined isogravimetrically from the slope of the lung weight-gain curve induced by a 7.5–mm Hg step elevation of the venous pressure for 10 min, as described previously (25, 36). These experiments were performed separately from the studies addressing $^{22}Na^+$ and [^{3}H]mannitol fluxes.

Statistical Treatment of Data

Numerical values are given as the mean ± SD. Intergroup differences were assessed by a factorial ANOVA with *post hoc* analysis with Fisher's least significant difference test, where P values < 0.05 were considered significant.

RESULTS

Thrombin Blocks Transepithelial Active Sodium Transport in Intact Lungs

Immediately after killing, the rabbit lungs had a calculated ELF volume of 0.66 ml (Table 1). By the time the isolated, perfused, and ventilated lungs had achieved steady-state conditions, they had acquired and retained an additional 1.75 ml of fluid. The fluid acquisition stabilized at this point, and remained stable over a 3-h period in untreated lungs. Therefore, under steady-state conditions, the isolated, ventilated, and perfused rabbit lungs had an ELF volume that was larger than the ELF volume observed in live animals. Most likely, there is a shift of fluid from the vascular and/or interstitial space into the alveolar space, which is an artifact of the lung isolation and perfusion. Thus, although our baseline ELF volumes are high, they remain stable between attainment of steady-state conditions, and the conclusion of the measurements in untreated lungs. After attainment of steady-state conditions, two fluid challenges, of 0.5 ml and 1 ml, respectively, were sequentially applied by ultrasonic nebulization (Figure 1) to an isolated, ventilated, and perfused rabbit lung. In healthy control lungs, the first challenge caused a transient 0.5-g increase in lung weight, which corresponds to deposition

of 0.5 ml of water into the lung (Figure 1A, *dashed box*). This fluid was cleared from the lungs within 15 min, after which lung weight returned to baseline. A second fluid challenge given 1 h later was resolved in 30–40 min (Figure 1A, *solid box*). Because twice the volume of fluid was applied in the second fluid challenge, compared with the first challenge, the magnitude of the lung weight gain and the duration of edema resolution after the second fluid challenge were larger than that observed after the first fluid challenge (Figure 1). Control lungs maintained at 37°C exhibited a nonsignificant net change in lung weight (0.16 ± 0.12 g loss; Figures 1 and 2A) over the experimental time course, while untreated lungs maintained at 4°C, where active transport was blocked, exhibited a net weight gain of 1.44 ± 0.30 g (Figure 2A).

After intravascular administration of thrombin (2.5 U/ml), an immediate but transient 2-fold increase in pulmonary arterial pressure (PAP) was observed (Figure 1B, *dotted box* on PAP trace). A simultaneous immediate, but transient, decrease in lung weight was also observed (Figure 1B, *dotted box* on lung weight trace). These effects are attributable to the potent vasoconstrictor properties of thrombin (23), which transiently reduced the vascular bed volume in the lung, hence the temporary decrease in lung weight. Ten to fifteen minutes after thrombin administration, both PAP and lung weight stabilized at their original values (Figure 1B). The lungs were then allowed to remain at steady-state for a further 20 min to ensure that the effects of the transient thrombin-induced vasoconstriction were lost before we started our measurements. A second fluid challenge was then applied, which caused a corresponding 1 g weight gain by the lung. In strong contrast to what we observed in our control lungs, this fluid was not cleared from the lungs (Figure 1B, *solid box*). Indeed, the weight of the thrombin-treated lungs gradually increased over the time-course of the experiment to a final value of 1.18 ± 0.24 g (Figures 1B and 2A). Amiloride (10 μM in the ELF) applied as a positive control for inhibition of active sodium clearance, also impaired fluid clearance from the lung, causing a net weight gain of 0.75 ± 0.23 g (Figure 2A). We then sought to establish where in the lungs this excess fluid was located.

Epithelial lining fluid volume was determined to investigate whether thrombin promoted retention of fluid in the alveolar space. During the preparation and initial perfusion of the isolated rabbit lungs, the lungs accumulated ~ 1.75 ml of fluid, after which the fluid retention stabilized (Table 1). This fluid retention is an artifact of the lung isolation and perfusion. In control lungs maintained at 37°C, the ELF volume was constant over the course of the experiment at ~ 2.46 ± 0.23 ml (Figure 2B). The ELF volume measurements corroborated our lung weight-gain data. When lungs were maintained at 4°C, the ELF volume increased to 3.97 ± 0.28 ml, indicating an average 1.51 ml increase in ELF volume. This extra fluid was attributable to fluid that was nebulized into the lung, but which could not be cleared, since active transport processes were shut down at 4°C. In the presence of amiloride, which also blocks active sodium transport and thereby fluid resorption, the ELF volume was also increased, albeit less dramatically, to 3.12 ± 0.12 ml (i.e., a 0.66-ml increase over control conditions). Similarly, treatment of lungs with thrombin caused a significant 0.84-ml increase in ELF volume (3.3 ± 0.28 ml) compared with control lungs. These data indicated that the bulk of the water that collected in the lungs after thrombin administration was located in the alveolar space. Since active sodium transport plays a key role in alveolar fluid clearance,

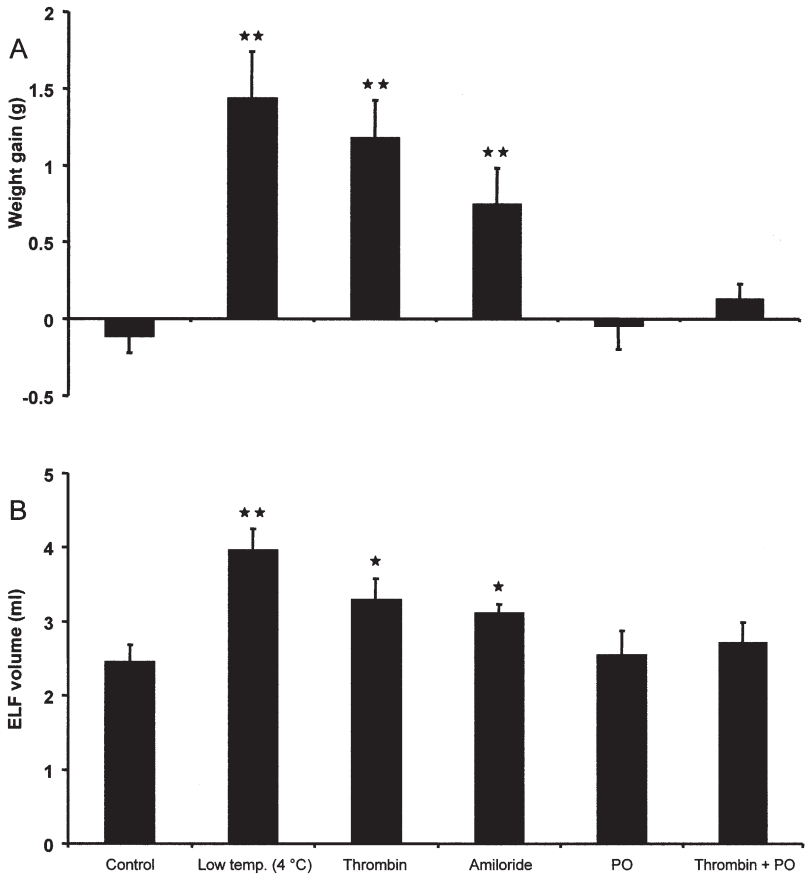

Figure 2. Thrombin blocks fluid clearance in isolated, ventilated, and perfused rabbit lungs. Fluid retention in the lungs was estimated from the net lung weight gain after fluid challenge, which was continuously monitored online throughout the experiment (*A*), and by determination of the ELF volume from BAL fluids (*B*), as described in MATERIALS AND METHODS. Lungs were either maintained at 37°C, or at 4°C (to block active transport). In additional experiments, thrombin (2.5 U/ml) was applied to the perfusate, or amiloride or phalloidin oleate (PO) was applied to the alveolar space, by nebulization (10 μM and 1 μM, respectively, final ELF concentration). In one set of experiments, PO and thrombin were applied sequentially as described in MATERIALS AND METHODS and in Figure 1A. Data represent the mean ± SD ($n = 6$ per group); $^*P < 0.01$, $^{**}P < 0.001$.

we investigated the effect of thrombin on transepithelial sodium transport in our lung model.

Transit of $^{22}Na^+$ and [^{3}H]mannitol from the alveolar compartment to the vascular compartment at 37°C and at 4°C permitted distinction between active and passive transport processes. This methodology has been described in detail previously (25). Original clearance curves depicting $^{22}Na^+$ transit from the alveolar to the vascular compartments in our isolated, ventilated, and perfused rabbit lung model are illustrated in Figure 3. At 37°C, $^{22}Na^+$ clearance is mediated by both active and passive transport processes, while at 4°C $^{22}Na^+$ clearance is attributable exclusively to passive transport processes, since active processes are shut down at this temperature (37). Thus, the fraction of $^{22}Na^+$ that is cleared from the lungs at 37°C but not cleared at 4°C is attributable to active processes. This active transport fraction is represented by the difference between the area above the curves for the warm (37°C) and cold (4°C) control lungs. These data are quantified in Figure 4. Passive paracellular permeability was unaffected under all experimental conditions (Figure 4, *open bars*). Therefore, the differences we observed in the $^{22}Na^+$ clearance were attributable to perturbations to active sodium transport (Figure 4, *closed bars*). After application of thrombin or amiloride, $^{22}Na^+$ clearance from the lung was reduced to 33.75 ± 2.56% and 32.50 ± 7.56% of the control values, respectively ($P < 0.01$ with versus control lungs). Our amiloride data are consistent with the observation that ~ 60% of the sodium transport channels in rabbit lungs are amiloride-sensitive (38). Together, these data indicate that the weight gains and ELF volume increases of the lung that are elicited by thrombin are most likely attributable to impaired transepithelial active sodium transport, which in turn blocks alveolar fluid clearance.

Our *in vitro* experiments in cell culture with endocytic inhibitors (*see below*) suggested that endocytosis played a key role in the thrombin-mediated effects that we observe on transepithelial active sodium transport. Hence, we applied the cell-permeable phalloidin analog, phalloidin oleate (1 μM in the ELF), in our isolated lung model. This compound potently inhibits endocytosis. Administration of phalloidin oleate before administration of thrombin blocked the thrombin-mediated effects on lung weight gain (0.13 ± 0.10 g; Figure 2A), ELF volume increase (2.72 ± 0.27 ml; Figure 2B) and on active sodium clearance (Figures 3 and 4). In the presence of phalloidin oleate, either with or without thrombin treatment, none of these parameters were significantly changed when compared with sham-treated, control lungs. Taken together, these data suggest that thrombin interferes with active transepithelial sodium transport in intact lungs and that this thrombin effect is linked to phalloidin-sensitive endocytic processes. Two important effector molecules of transepithelial active sodium transport are ENaC (39) and Na^+,K^+-ATPase (40), although potassium and other ion channels could also influence this process (41). It seemed likely that thrombin stimulated the endocytosis of one or more of these effector molecules. To verify and further elaborate on these findings, studies in cultured lung epithelial cells were undertaken.

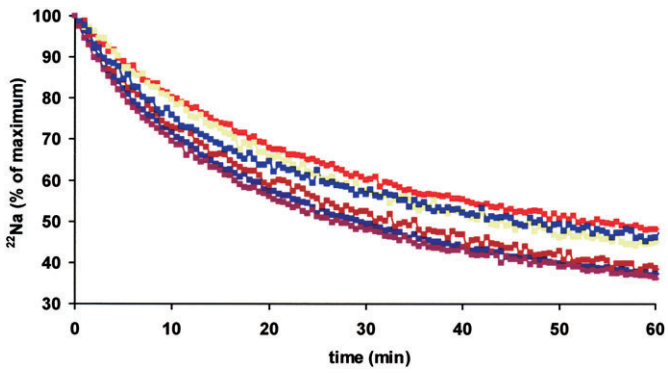

Figure 3. Thrombin blocks sodium transport in an isolated, ventilated, and perfused rabbit lung model. After deposition of radioactive tracers (^{22}NaCl and [^{3}H]mannitol) into the lung by ultrasonic nebulization, ^{22}Na clearance from the lung was continuously monitored for 60 min. Before application of tracers, lungs received different treatments, indicated in the scheme in Figure 1. Sham-treated lungs (receiving 5 ml perfusate solution instead of thrombin) were maintained at either at 37°C (*blue*) or 4°C (*red*). Alternatively, thrombin (2.5 U/ml in 5 ml perfusate solution; *yellow*) or amiloride (10 μM final concentration in the ELF; *light blue*) had been applied to lungs maintained at 37°C. In other cases, phalloidin oleate (1 μM final concentration in the ELF) was applied to lung before sham (receiving 5 ml perfusate; *magenta*) or thrombin (2.5 U/ml in 5 ml perfusate; *brown*) treatment. For the purposes of clarity, standard deviations (which were always < 2.2%, with the exception of control lungs and amiloride-treated lungs at 37°C, which were 3% and 5%, respectively) have been omitted. However, they are incorporated into the analyses of these data in Figure 4.

Effects of Thrombin on Whole-Cell Current in A549 and ATII Cells

In the whole-cell mode, A549 cells exhibited inward rectifying currents carried by Na^+ as reported previously (32). Preincubation the cells with thrombin (2.5 U/ml) for 1 h did not change the whole-cell current (Figures 5A and 5B; $n = 5$). When the pretreated cells were additionally superfused with amiloride (10 μM), a significant reduction of the inward Na^+ current to 51 ± 11% (at −100 mV) and shift of the reversal potential to +41 mV was observed. Application of 10 μM amiloride to control untreated cells caused a similar effect on the inward Na^+ current. The effect of thrombin on amiloride-sensitive sodium current was also investigated in ATII cells. With the use of bath-2 solution and whole-cell pipette-2 solution, the families of currents (Figures 5C and 5D) elicited by voltage-stepping protocol evoked essentially linear current–voltage relationship. A 1-h exposure to 2.5 U/ml thrombin resulted in no significant change in whole-cell current (Figures 5C and 5D). Consistent with previous reports (42), amiloride (10 μM) significantly inhibited the currents (Figures 5D and 5E). Thus, thrombin had no effect on the whole-cell current in A549 and ATII cells. Since preincubation of the cells with thrombin for 1 h did not change the whole cell current (neither inward [Na^+] nor outward [K^+] currents), we suspected that thrombin mediated changes to sodium pump activity, and did not alter sodium and potassium channel activity.

Thrombin Blocks Na^+,K^+-ATPase Activity in A549 and ATII Cells by Promoting Na^+,K^+-ATPase Endocytosis in an ROS- and PKC-ζ–Dependent Manner

The activity of Na^+,K^+-ATPase was estimated from ouabain-sensitive $^{86}Rb^+$ uptake. Thrombin (2.5–10 U/ml) caused a significant ($P = 0.01$–0.001), dose-dependent decrease in ouabain-sensitive $^{86}Rb^+$ uptake by A549 cells, and thus Na^+,K^+-ATPase activity, abrogating ~ 60% of the activity at 10 U/ml, in comparison to untreated cells, or cells pretreated for 30 min with phalloidin oleate (1 μM; Figure 6A). The thrombin concentration that was applied in the isolated, ventilated, and perfused rabbit lungs (2.5 U/ml) fell within this range. At concentrations of 0.5 U/ml and 0.05 U/ml, thrombin also inhibited Na^+,K^+-ATPase function in A549 cells in comparison to cells pretreated for 30 min with phalloidin oleate (1 μM); however, these differences were not statistically significant ($P = 0.22$ and 0.54, respectively; Figure 6A). No changes were observed in ouabain-insensitive $^{86}Rb^+$ uptake

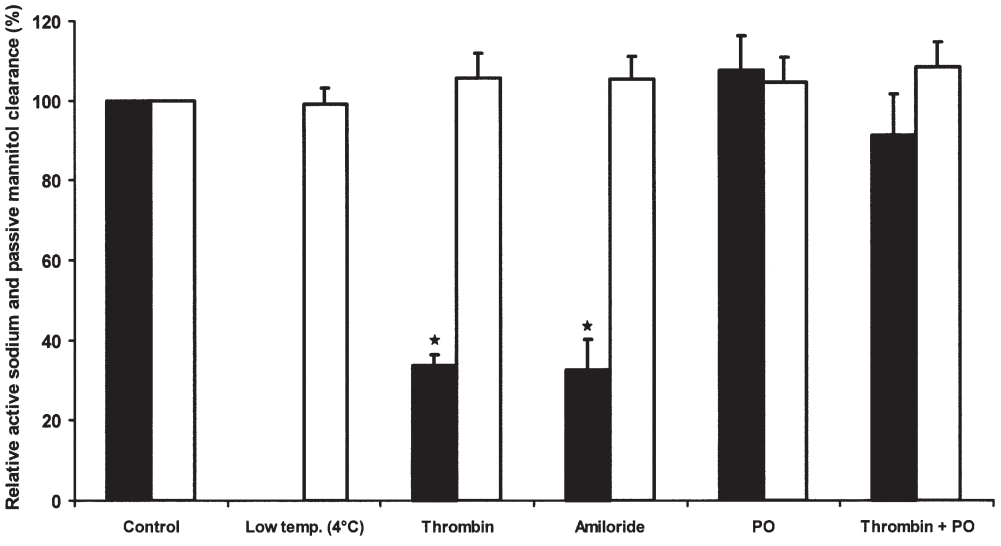

Figure 4. Thrombin blocks active sodium transport without altering passive paracellular epithelial permeability of intact lungs. Active ^{22}Na transport (*solid bars*) was quantified from the data in Figure 3 as described in MATERIALS AND METHODS. The active ^{22}Na transport in untreated lungs maintained at 37°C was set at 100%, with the active ^{22}Na transport in treated lungs expressed relative to this control value. Passive [^{3}H]mannitol flux (*open bars*) was monitored by liquid scintillation counting of perfusate samples taken at discrete time intervals after nebulization of the [^{3}H]mannitol tracer to the lungs, as described in MATERIALS AND METHODS. The passive [^{3}H]mannitol flux in untreated lungs maintained at 37°C was set at 100%, and mannitol flux in treated lungs was expressed relative to this control value. No active transport occurs at 4°C, hence there is no value for this parameter in the figure. *Bars* represent the mean ± SD ($n = 6$ for all groups); *$P < 0.001$. PO, phalloidin oleate.

(data not shown), suggesting a specific effect on the Na^+,K^+-ATPase. Since A549 cells do not form tight transporting monolayers (43), we conducted our subsequent experiments in both A549 and primary ATII cells in parallel. This thrombin-mediated effect was blocked by preincubation of A549 (Figure 6B) and ATII (Figure 6C) cells with DPI, a potent though nonspecific inhibitor of NAD(P)H oxidase, but not by the mitochondrial NADH dehydrogenase inhibitor rotenone (Figures 6B and 6C). This thrombin-mediated effect was also dependent upon PKC activity, in particular PKC-ζ, since both cell-permeable myristoylated

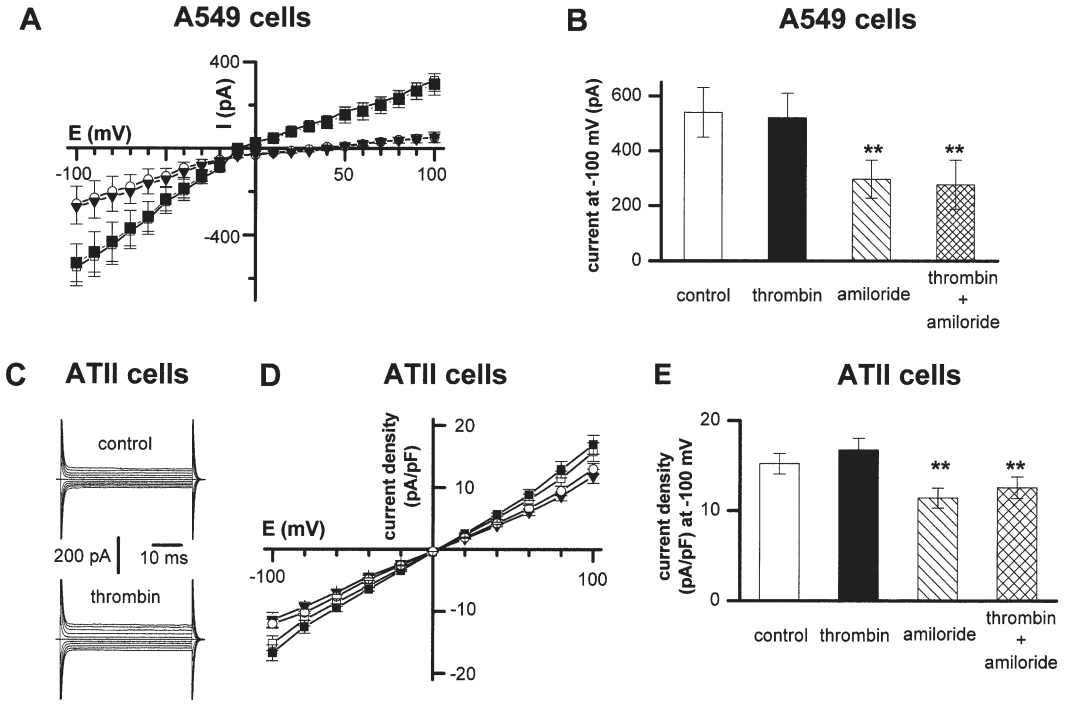

Figure 5. Effects of thrombin on whole-cell current in A549 and ATII cells. (*A*) Averaged whole-cell I-V plots of whole-cell current in control (*open squares*) and after preincubation with 2.5 U/ml thrombin (*filled squares*). The effects of amiloride (*circles*) and thrombin plus amiloride (*triangles*) on steady-state currents are also depicted. Amiloride or thrombin plus amiloride-sensitive currents were obtained by subtracting residual current from total current as described in MATERIALS AND METHODS. Values represent mean ± SD ($n = 5$). (*B*) Summarized data of whole-cell current elicited by a test potential at −100 mV in control and after perfusion with thrombin (2.5 U/ml), amiloride (10 μM), or thrombin plus amiloride ($n = 5$). **$P < 0.01$ for comparison to control. (*C*) Typical whole-cell Na^+ currents recorded in ATII cells in the absence (*top*) or after pretreatment with 2.5 U/ml thrombin (*bottom*). (*D*) Mean current density versus voltage relationship for control (*open squares*) and thrombin-pretreated (2.5 U/ml; *filled squares*) ATII cells. The effects of amiloride (10 μM; *triangles*) alone or thrombin (2.5 U/ml) plus amiloride (10 μM; *circles*) are also illustrated ($n = 5$). (*E*) Summarized data of whole-cell current density elicited by a test potential at −100 mV in the cell treatments described in *D*. **$P < 0.01$ compared with control.

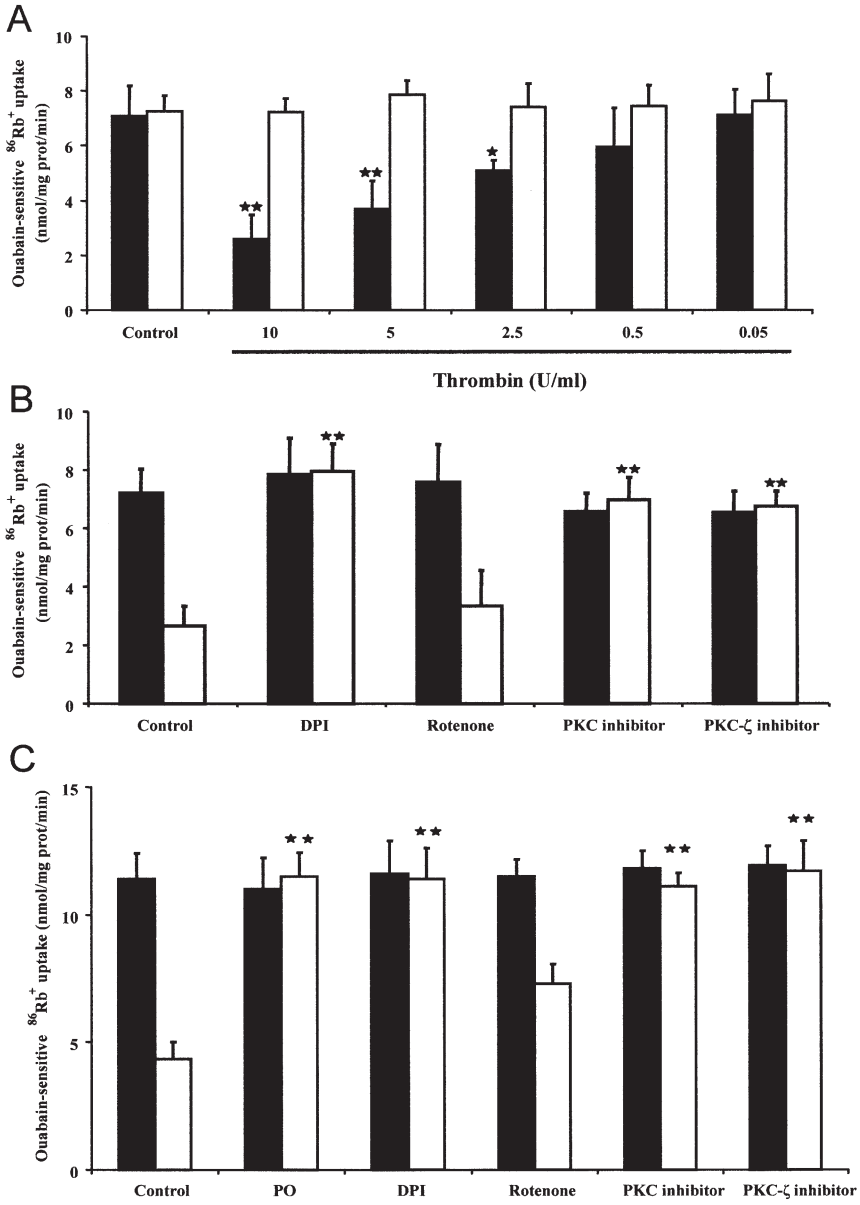

Figure 6. Thrombin blocks ouabain-sensitive $^{86}Rb^+$ uptake by A549 and ATII cells in an endocytosis-dependent manner: impact of ROS and PKC-ζ. (*A*) The uptake of $^{86}Rb^+$ by A549 and ATII cells was assessed in the presence of various concentrations of thrombin (0.05–10 U/ml), or in serum-free media alone (control), after preincubation (30 min) either in the absence or presence of 1 μM phalloidin oleate in 0.1% (vol/vol) DMSO (*open bars*) in serum-free media. The uptake of $^{86}Rb^+$ by A549 (*B*) and ATII (*C*) cells was assessed in the absence (*closed bars*) or presence (*open bars*) of 10 U/ml thrombin, after preincubation (15 min) either with 0.1% (vol/vol) DMSO in serum-free media alone, or with DPI (5 μM), rotenone (1 μM), myristoylated PKC general antagonist peptide (30 μM), or myristoylated PKC-ζ antagonist peptide (15 μM), all dissolved in 0.1% (vol/vol) DMSO (*open bars*) in serum-free media. Each *bar* represents the mean ± SD ($n = 6$, for each experimental condition). *$P < 0.05$, **$P < 0.01$.

pseudosubstrate peptide antagonists of PKC and specifically PKC-ζ also restored ouabain-sensitive $^{86}Rb^+$ uptake to control values in A549 (Figure 6B) and ATII (Figure 6C) cells.

Thrombin Promotes Endocytosis of Na^+,K^+-ATPase, but Does Not Alter ENaC Cell-Surface Expression

Cell-surface expression of Na^+,K^+-ATPase was significantly ($P < 0.001$) reduced after treatment of A549 (Figure 7A) or ATII (Figures 7B and 7C) cells with thrombin (2.5 U/ml), when compared with untreated cells. In contrast, thrombin did not alter cell-surface expression of ENaC α or β subunits (Figures 7A–7C). The bands illustrated in Figure 7 were the only bands observed in the vicinity of the molecular mass of interest. These data suggest that thrombin can reduce cell-surface expression of Na^+,K^+-ATPase, thereby regulating its activity at the cell surface. Preincubation of A549 (Figure 7A) and ATII (Figure 7B) cells with the endocytosis inhibitor phalloidin oleate (1 μM, 30 min) abrogated the thrombin-mediated reduction in cell-surface expression of Na^+,K^+-ATPase. Thus, thrombin can promote the endocytosis of the Na^+,K^+-ATPase. In ATII cells, we also demonstrated that this thrombin-mediated endocytosis of Na^+,K^+-ATPase was inhibited in the presence of a cell-permeable myristoylated pseudosubstrate peptide antagonist of PKC-ζ (Figure 7B). In addition, DPI significantly ($P < 0.01$) blocked the thrombin-mediated endocytosis of Na^+,K^+-ATPase (Figure 7C), while rotenone slightly, although nonsignificantly ($P > 0.05$), blocked this thrombin-mediated effect (Figure 7C).

Thrombin Increases Endothelial Permeability in Intact Lungs

In control isolated, ventilated, and perfused rabbit lungs maintained at 37°C, no change in endothelial permeability was observed, as indicated by essentially unchanged capillary filtration coefficient ($K_{f,c}$) values determined at 40, 60, and 120 min after the lungs reached steady-state equilibrium. The $K_{f,c}$ values remained constant around 0.0095 ± 0.001 ml/min/cm H_2O/g dry weight (Figure 8). Lungs maintained at 4°C exhibited no perturbations to endothelial permeability over the 120-min time-course (Figure 8). Similarly, no changes in $K_{f,c}$ were observed when lungs were treated with amiloride (10 μM). In contrast to these data, thrombin (2.5 U/ml in the perfusate) caused a significant

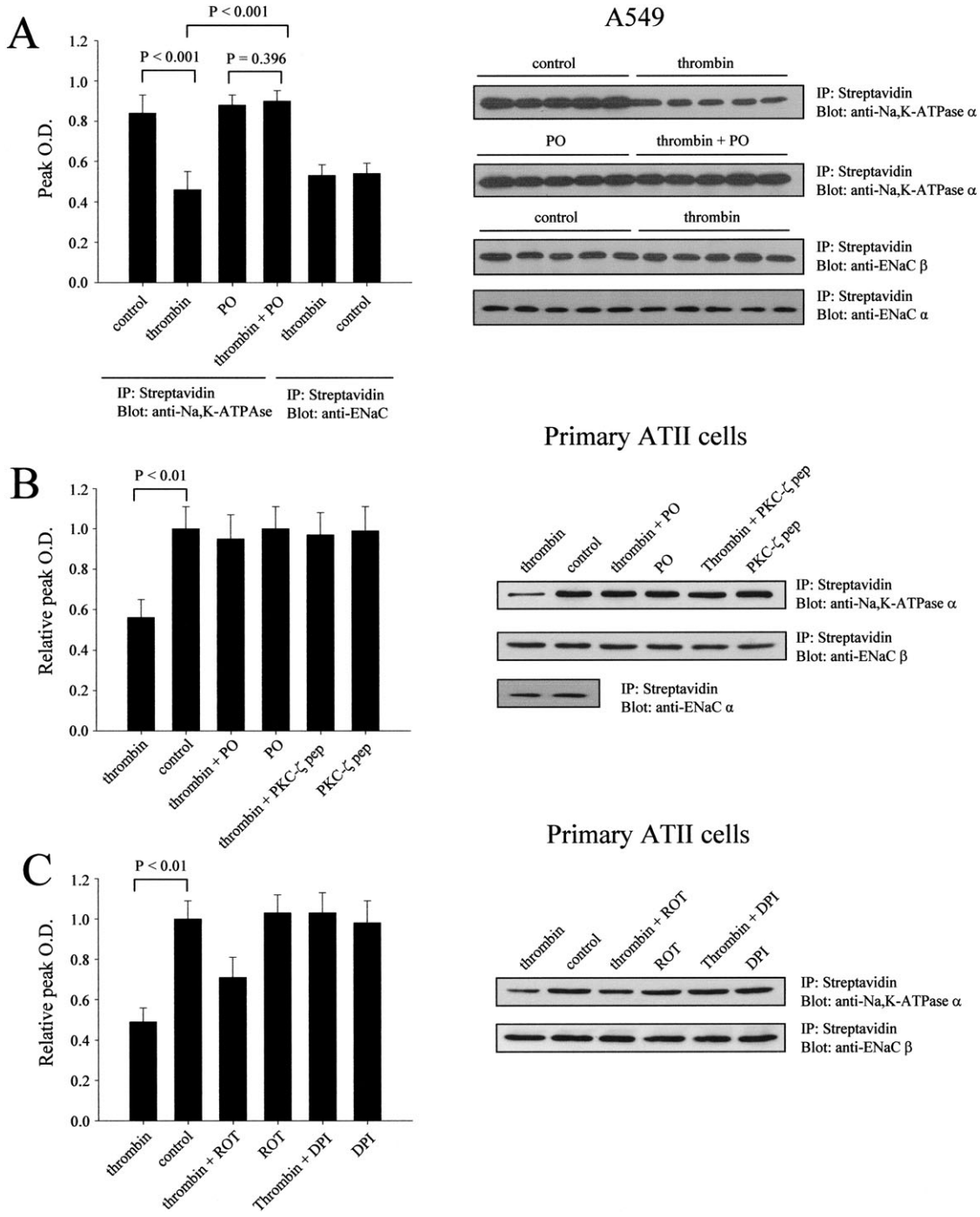

Figure 7. Thrombin downregulates cell-surface expression of Na^+,K^+-ATPase by endocytosis in a ROS- and PKC-ζ–dependent manner. (*A*) Subconfluent monolayers of A549 cells were sham-treated, or treated with thrombin (2.5 U/ml) for 1 h, either with or without a 30-min preincubation with PO as described in the legend to Figure 6. Biotinylated cell-surface proteins were isolated by a streptavidin-agarose pulldown, and were resolved by SDS-PAGE and transferred to a PVDF membrane. Membranes were probed for Na^+,K^+-ATPase α1 (112 kD) and ENaC α (125 kD) and β (95 kD) subunits as described in MATERIALS AND METHODS. Bands illustrated were the only bands observed in the vicinity of the molecular mass of interest. A densitometric analysis of the streptavidin pulldowns is illustrated on the *left-hand side* of the panel, while the blots are illustrated on the *right-hand side*. Data represent the mean ± SD (n = 5 per group). Primary ATII cells were similarly treated (*B* and *C*). In the case of primary cells, densitometric analyses are expressed (for Na^+,K^+-ATPase only), as relative peak optical density (OD), normalized for the untreated (control) cells. In addition to PO, primary ATII cells were also pretreated with a myristoylated PKC-ζ antagonist peptide (PKC-ζ pep), ROT, or DPI, as described in the legend to Figure 6. Representative blots from streptavidin pulldowns are illustrated on the *right-hand side*. Data represent the mean ± SD (n = 3 per group).

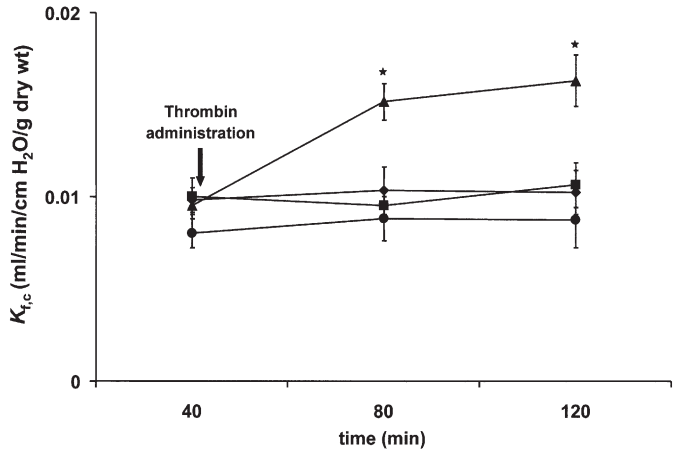

Figure 8. Thrombin increases endothelial permeability of intact lungs. Endothelial permeability was assessed from capillary filtration coefficients ($K_{f,c}$) determined for lungs maintained at 37°C (*squares*) or at 4°C (*circles*). Coefficients were also determined after administration of thrombin (2.5 U/ml in the perfusate; *triangles*) or amiloride (10 μM in the ELF; *diamonds*) to lungs maintained at 37°C. Data represent the mean ± SD ($n = 4$ per group). *$P < 0.05$.

($P < 0.01$) increase in the endothelial permeability, increasing the $K_{f,c}$ by 50%, to 0.0163 ± 0.0014 ml/min/cm H_2O/g dry weight (Figure 8).

DISCUSSION

Coagulation factors, in particular thrombin, have been implicated both as pathogenic (8) and diagnostic (44) factors in ALI/ARDS. Thrombin has been identified as a factor that can promote edema formation either directly, by increasing endothelial permeability for fluids and large solutes (19); or indirectly, by inducing microvascular coagulopathy and DIC (13, 14, 22). While several studies have correlated elevated procoagulant activity of BAL fluids and plasma with the development of ALI/ARDS (9–11), and the ability of thrombin to provoke alveolar edema has been experimentally demonstrated (45), no study to date has investigated the impact of thrombin on key properties of the alveolar epithelium with respect to its function in the resolution of alveolar edema.

To address this question, we employed an isolated, ventilated, and perfused rabbit lung model. This model was attractive for several reasons. It is a blood-free system, and it was therefore possible to explore the effects of thrombin applied to the vascular compartment, in the absence of plasma peptidase inhibitors. Furthermore, any involvement of the coagulation pathway (such as microvascular coagulopathy) in the persistence of alveolar edema in our model was excluded. This model also facilitates online real-time tracing of sodium efflux from the lung. However, this model is not without its drawbacks, most notably an elevated steady-state ELF volume, reflecting a shift of fluid from the vascular and/or interstitial space into the alveolar space. This is an artifact of the lung isolation and perfusion, perhaps resulting from severing of the lymphatic vessels that would drain excess interstitial fluid. In spite of this, however, we do not believe that this artifact calls into question the validity of the conclusions we draw from our investigations, since measurements were always made after attainment of steady-state conditions, and the thrombin-induced effects yielded significantly elevated ELF volumes compared with those of control, untreated lungs. Furthermore, these thrombin-induced effects could be effectively blocked by a variety of interventions, which maintained the baseline ELF volume equivalent to that observed in control, untreated lungs, both in the absence and presence of thrombin.

Our data indicated that thrombin, applied to the vascular space, caused a pronounced increase in both lung weight and ELF volume after a fluid challenge. These increases were not observed in sham-treated lungs that received the same fluid challenge, indicating that thrombin could interfere with alveolar fluid clearance. Fluid clearance from the alveolar compartment is undertaken primarily by two sodium transporters: ENaC (39) and Na^+,K^+-ATPase (40, 46), of which the α1 and α2 subunits have recently been described to play a synergistic role (47). Furthermore, other ion channels, including chloride and potassium channels, can influence this fluid clearance (41). Both ENaC and Na^+,K^+-ATPase act in concert to drive active transepithelial sodium transport, and hence the transport of water, out of the alveolar space, into the interstitium. This active transepithelial sodium transport plays a pivotal role in the resolution of pulmonary edema (6, 7). Administration of thrombin to the vascular compartment caused a significant decrease in active ^{22}Na clearance from the lungs, while paracellular permeability remained unchanged. Therefore, the thrombin-mediated block of edema resolution results, at least in part, from blocked active transepithelial sodium transport. It followed that thrombin most likely influenced the activity of either Na^+,K^+-ATPase or ENaC, or both of these molecules. Therefore, we further investigated the influence of thrombin on these sodium transport systems in isolated epithelial cells.

Thrombin had no effect on the function of amiloride-sensitive sodium channels such as ENaC in A549 human lung epithelial cells or in primary murine alveolar type II cells. In contrast, a 30-min preincubation with thrombin dramatically decreased Na^+,K^+-ATPase activity, indicating that thrombin most likely impaired active transepithelial sodium transport in the lung by blocking Na^+,K^+-ATPase activity. The activity of Na^+,K^+-ATPase can be regulated at both the transcriptional and post-translational levels. Genes encoding the constituent subunits of Na^+,K^+-ATPase are responsive to steroid and peptide hormone signaling pathways. Angiotensin II upregulates Na^+,K^+-ATPase α subunit expression, in a phosphatidyl-inositol-3-kinase and p42/44 mitogen-activated protein kinase signaling-dependent manner (48), while follicle-stimulating hormone upregulates Na^+,K^+-ATPase β subunit mRNA levels (49). However, the short time-frame of our experiments (30 min–2 h) essentially precludes a transcriptional effect. Additional regulatory mechanisms have been identified that occur rapidly (within minutes) in Na^+-transporting renal and lung epithelial cells. In the lung, Na^+,K^+-ATPase density on the plasma membrane can be increased by activation of the D_1 dopamine receptor, which recruits and translocates Na^+,K^+-ATPase from intracellular pools to the basolateral membrane (50, 51). This recruitment is mediated by protein phosphatase 2A (50) and two PKC isoforms, PKC-δ and PKC-ϵ (51). Similarly, 3,3′,5-triiodo-L-thyronine can also induce cell-surface expression of Na^+,K^+-ATPase by a phosphoinositide-3-kinase– and Src kinase–dependent pathway (52). Conversely, other extracellular signals such as hypoxia can induce endocytosis of Na^+,K^+-ATPase, thereby reducing plasma membrane density, and hence Na^+,K^+-ATPase activity, at the cell surface (46). This effect is mediated by a different PKC isoform, PKC-ζ and ROS (35). Indeed, when directly investigated in the present study, we found that thrombin reduced the cell-surface density of Na^+,K^+-ATPase, which may well explain the reduced Na^+,K^+-ATPase activity that we observed in our $^{86}Rb^+$ uptake assays in A549 and ATII cells.

We proposed that thrombin-stimulated endocytosis of Na^+,K^+-ATPase might explain the thrombin-induced reductions

in Na^+,K^+-ATPase density at the cell surface. To investigate Na^+,K^+-ATPase endocytosis, we employed the membrane-permeable phalloidin analog, phalloidin oleate, a potent F-actin–binding agent that prevents F-actin ↔ G-actin conversion, thereby preventing endocytic processes. Phalloidin oleate is a very specific inhibitor of actin reorganization, and affects all processes that depend on actin mobility, such as endocytosis (53). Although phalloidin and its derivatives are relatively toxic, we have employed this inhibitor at concentrations that have previously been shown to prevent hypoxia-mediated endocytosis of Na^+,K^+-ATPase without adversely effecting cell viability (54). In the presence of phalloidin oleate, thrombin could not induce any reduction in the cell-surface density of Na^+,K^+-ATPase. Similarly, in the presence of phalloidin oleate, thrombin had no effect on $^{86}Rb^+$ uptake by A549 or ATII cells. Thus, our data indicated that thrombin can promote the endocytosis of Na^+,K^+-ATPase from the cell surface. Indeed, in our isolated lung model, prenebulization of the endocytosis inhibitor phalloidin oleate to the alveolar compartment, 30 min before the application of thrombin intravascularly, protected the lung from the thrombin-induced fluid-clearance block. These phalloidin oleate–treated lungs were able to effect edema resolution at a rate comparable to that of control lungs that had not been treated with thrombin. Since the phalloidin oleate was applied to the alveolar space, and since the phalloidin oleate blocked thrombin-mediated effects on in Na^+,K^+-ATPase cell-surface density, and $^{86}Rb^+$ uptake by A549 or ATII cells in culture, we propose that phalloidin oleate also prevents the thrombin-induced reduction in cell-surface density of Na^+,K^+-ATPase in the epithelial layer of the isolated rabbit lung.

Hypoxia can also promote the endocytosis of Na^+,K^+-ATPase (46) in a ROS-dependent and PKC-ζ–dependent manner (35). Because thrombin signaling both induces ROS production in endothelial cells (55) and induces PKC-ζ in endothelial cells (56), we reasoned that ROS and PKC-ζ might be involved in the signal transduction pathway elicited by thrombin. To address this possibility, we employed two inhibitors of ROS generation, DPI, an inhibitor of NAD(P)H oxidase, and rotenone, an inhibitor of mitochondrial NADH dehydrogenase, in our $^{86}Rb^+$ uptake studies. Indeed, DPI blocked the thrombin-mediated inhibition of $^{86}Rb^+$ uptake, however, rotenone did not. Together, these data would argue in favor of a role for flavoenzyme (i.e., NAD[P]H oxidase)–, but not mitochondrial NADH-dehydrogenase–generated ROS in the thrombin signaling pathway. However, DPI is an unspecific inhibitor of ROS production, since it inhibits nonmitochondrial NAD(P)H oxidases, and, at the concentrations employed in the present study it can also inhibit production of superoxide and H_2O_2 by mitochondria, the major source of cellular ROS, probably by inhibiting NADH-ubiquinone oxidoreductase (complex I) (57), together with various nitric oxide synthases (58). Thus, while we present evidence here that implicates ROS in the thrombin-signaling pathway, their source remains unclear.

Given that ROS can activate PKC (59), and the demonstrated role for PKC in coupling hypoxia to Na^+,K^+-ATPase activity, we also explored a role for PKC in the thrombin signaling pathway. Both a broad-spectrum cell-permeable pseudosubstrate inhibitor of PKCs, and a specific cell-permeable pseudosubstrate inhibitor of PKC-ζ completely blocked the thrombin-mediated inhibition of $^{86}Rb^+$ uptake. Since phosphorylation of the Na^+,K^+-ATPase α subunit can trigger endocytosis of Na^+,K^+-ATPase (60), and since this phosphorylation can be undertaken by various PKC isoforms (61), we propose a model where thrombin, signaling through protease-activated receptors, induces intracellular ROS generation, which then activates PKC-ζ. PKC-ζ subsequently promotes Na^+,K^+-ATPase phosphorylation, promoting its endocytosis and hence loss of activity at the cell surface. This loss of Na^+,K^+-ATPase activity would have serious implications for fluid balance dynamics in the lung.

While thrombin-induced reductions in Na^+,K^+-ATPase activity play a key role in preventing edema resolution, the effects of thrombin on edema persistence are not limited to Na^+,K^+-ATPase–mediated processes. In our isolated lung model, we have observed that the net weight gain by thrombin-treated lungs was in excess of the weight of fluid that we applied to the lungs with fluid challenges. Thus, after thrombin application, additional fluid was able to leak into the extravascular compartments. This would suggest that additional thrombin-mediated perturbations to alveolar–capillary barrier integrity occur. This barrier is formed by two independent barriers: the vascular endothelium, and the alveolar epithelium. We have already documented in this study that thrombin does not perturb the integrity of the alveolar epithelium, since passive flux of small solutes was unchanged, comparing control lungs to those treated with thrombin. In contrast to these data, thrombin treatment did increase the capillary filtration coefficients, and thus vascular permeability. These data are consistent with other studies documenting thrombin-mediated changes to endothelial barrier integrity *in vitro* (18). Thrombin can also increase lung epithelial permeability in live animals; however, this permeability increase was dependent on the activation of intravascular coagulation (22). Since our model is a blood-free system, coagulation-dependent perturbations to epithelial permeability are unlikely. However, the development of alveolar edema in the presence of an apparently intact alveolar membrane is well described (62, 63), perhaps due to the substantially elevated interstitial hydrostatic pressure (64) that results from interstitial fluid loading from the vascular space, which may force fluid across the alveolar epithelium (65). In our isolated lung model, in the presence of the endocytosis inhibitor phalloidin oleate (which fully maintains active sodium transport, even in the presence of thrombin) a 0.2-g weight-gain by the lungs (paralleled by a $\sim$ 0.17-ml ELF volume increase) was still observed after thrombin application. This weight gain could not be attributed to blocked active transepithelial sodium transport. We believe that this additional fluid gain by the lungs resulted from thrombin-induced increased endothelial permeability.

Taken together, our data suggest that the fluid retention that we observe in thrombin-treated lungs is probably the sum of two independent processes that occur concurrently. First, thrombin causes an increase in the endothelial permeability, and thus promotes alveolar flooding with fluid from the vascular space. Second, thrombin inhibits active transepithelial sodium transport (and thus transport of fluid) out of the alveolar space, a hitherto unrecognized property of this protease. This causes retention of fluid by the lung. Both of these effects combine to favor the formation and persistence of alveolar edema.

Conflict of Interest Statement: I.V. does not have a financial relationship with a commercial entity that has an interest in the subject of this paper. R.E.M. does not have a financial relationship with a commercial entity that has an interest in the subject of this paper. A.O. does not have a financial relationship with a commercial entity that has an interest in the subject of this paper. M.K. does not have a financial relationship with a commercial entity that has an interest in the subject of this paper. M.G.K. does not have a financial relationship with a commercial entity that has an interest in the subject of this paper. H.A.G. receives grant and contract support from Pfizer Ltd. In addition, he serves on an advisory board of Pfizer, Schering, and Altana Pharma. F.G. receives grant and contract support from Pfizer Ltd. and Altana Pharma AG. In addition, he serves on an advisory board of Altana Pharma AG. W.S. receives grant and contract support by the following companies: Schering AG, Pfizer Ltd., Altana Pharma AG, Lung Rx, Myogen.

Acknowledgments: The authors thank Professors Jacob I. Sznajder and David H. Rutschman for constructive criticisms, Gerd Weigand for performing the radiodosimetry, and Dr. Patrick Bulau and Sebastian Rummel for outstanding support.

References

1. Ware LB, Matthay MA. The acute respiratory distress syndrome. *N Engl J Med* 2000;342:1334–1349.
2. Frutos-Vivar F, Nin N, Esteban A. Epidemiology of acute lung injury and acute respiratory distress syndrome. *Curr Opin Crit Care* 2004;10:1–6.
3. Mehta D, Bhattacharya J, Matthay MA, Malik AB. Integrated control of lung fluid balance. *Am J Physiol Lung Cell Mol Physiol* 2004;287: L1081–L1090.
4. Matthay MA, Wiener-Kronish JP. Intact epithelial barrier function is critical for the resolution of alveolar edema in humans. *Am Rev Respir Dis* 1990;142:1250–1257.
5. Sznajder JI. Strategies to increase alveolar epithelial fluid removal in the injured lung. *Am J Respir Crit Care Med* 1999;160:1441–1442.
6. Matthay MA. Alveolar fluid clearance in patients with ARDS: does it make a difference? *Chest* 2002;122:340S–343S.
7. Sznajder JI. Alveolar edema must be cleared for the acute respiratory distress syndrome patient to survive. *Am J Respir Crit Care Med* 2001; 163:1293–1294.
8. Idell S. Coagulation, fibrinolysis, and fibrin deposition in acute lung injury. *Crit Care Med* 2003;31:S213–S220.
9. Gunther A, Mosavi P, Heinemann S, Ruppert C, Muth H, Markart P, Grimminger F, Walmrath D, Temmesfeld-Wollbruck B, Seeger W. Alveolar fibrin formation caused by enhanced procoagulant and depressed fibrinolytic capacities in severe pneumonia: comparison with the acute respiratory distress syndrome. *Am J Respir Crit Care Med* 2000;161:454–462.
10. Idell S, James KK, Levin EG, Schwartz BS, Manchanda N, Maunder RJ, Martin TR, McLarty J, Fair DS. Local abnormalities in coagulation and fibrinolytic pathways predispose to alveolar fibrin deposition in the adult respiratory distress syndrome. *J Clin Invest* 1989;84:695–705.
11. Gando S, Nanzaki S, Morimoto Y, Kobayashi S, Kemmotsu O. Systemic activation of tissue-factor dependent coagulation pathway in evolving acute respiratory distress syndrome in patients with trauma and sepsis. *J Trauma* 1999;47:719–723.
12. Seeger W, Hubel J, Klapettek K, Pison U, Obertacke U, Joka T, Roka L. Procoagulant activity in bronchoalveolar lavage of severely traumatized patients–relation to the development of acute respiratory distress. *Thromb Res* 1991;61:53–64.
13. Ruf W, Riewald M. Tissue factor-dependent coagulation protease signaling in acute lung injury. *Crit Care Med* 2003;31:S231–S237.
14. ten Cate H, Schoenmakers SH, Franco R, Timmerman JJ, Groot AP, Spek CA, Reitsma PH. Microvascular coagulopathy and disseminated intravascular coagulation. *Crit Care Med* 2001;29:S95–S97. (discussion S97–8).
15. Johnson K, Choi Y, DeGroot E, Samuels I, Creasey A, Aarden L. Potential mechanisms for a proinflammatory vascular cytokine response to coagulation activation. *J Immunol* 1998;160:5130–5135.
16. Laterre PF, Wittebole X, Dhainaut JF. Anticoagulant therapy in acute lung injury. *Crit Care Med* 2003;31:S329–S336.
17. Matthay MA, Zimmerman GA, Esmon C, Bhattacharya J, Coller B, Doerschuk CM, Floros J, Gimbrone MA Jr, Hoffman E, Hubmayr RD, *et al.* Future research directions in acute lung injury: summary of a National Heart, Lung, and Blood Institute working group. *Am J Respir Crit Care Med* 2003;167:1027–1035.
18. Kawkitinarong K, Linz-McGillem L, Birukov KG, Garcia JG. Differential regulation of human lung epithelial and endothelial barrier function by thrombin. *Am J Respir Cell Mol Biol* 2004;31:517–527.
19. Garcia JG, Siflinger-Birnboim A, Bizios R, Del Vecchio PJ, Fenton JW II, Malik AB. Thrombin-induced increase in albumin permeability across the endothelium. *J Cell Physiol* 1986;128:96–104.
20. Essler M, Amano M, Kruse HJ, Kaibuchi K, Weber PC, Aepfelbacher M. Thrombin inactivates myosin light chain phosphatase via Rho and its target Rho kinase in human endothelial cells. *J Biol Chem* 1998;273:21867–21874.
21. Garcia JG, Verin AD, Schaphorst K, Siddiqui R, Patterson CE, Csortos C, Natarajan V. Regulation of endothelial cell myosin light chain kinase by Rho, cortactin, and p60(src). *Am J Physiol* 1999;276:L989–L998.
22. Cooper JA, Feustel PJ, Line BR, Malik AB. Pulmonary epithelial clearance of 99mTc-DTPA after thrombin-induced pulmonary microembolism. *Am Rev Respir Dis* 1986;134:734–738.
23. Horgan MJ, Fenton JW II, Malik AB. Alpha-thrombin-induced pulmonary vasoconstriction. *J Appl Physiol* 1987;63:1993–2000.
24. Vadász I, Morty RE, Olschewski A, Kohstall MG, Grimminger F, Ghofrani HA, Seeger W. Alpha-thrombin inhibits alveolar fluid reabsorption by blocking Na,K-ATPase function in the lung [abstract]. *Proc Am Thoracic Soc* 2005;2:A838.
25. Vadász I, Morty RE, Kohstall MG, Olschewski A, Grimminger F, Seeger W, Ghofrani HA. Oleic acid inhibits alveolar fluid reabsorption: a role in acute respiratory distress syndrome? *Am J Respir Crit Care Med* 2005;171:469–479.
26. Ghofrani HA, Kohstall MG, Weissmann N, Schmehl T, Schermuly RT, Seeger W, Grimminger F. Alveolar epithelial barrier functions in ventilated perfused rabbit lungs. *Am J Physiol Lung Cell Mol Physiol* 2001; 280:L896–L904.
27. Nielson DW. Electrolyte composition of pulmonary alveolar subphase in anesthetized rabbits. *J Appl Physiol* 1986;60:972–979.
28. Effros RM, Feng NH, Mason G, Sietsema K, Silverman P, Hukkanen J. Solute concentrations of the pulmonary epithelial lining fluid of anesthetized rats. *J Appl Physiol* 1990;68:275–281.
29. Hamill OP, Marty A, Neher E, Sakmann B, Sigworth FJ. Improved patch-clamp techniques for high-resolution current recording from cells and cell-free membrane patches. *Pflugers Arch* 1981;391:85–100.
30. Corti M, Brody AR, Harrison JH. Isolation and primary culture of murine alveolar type II cells. *Am J Respir Cell Mol Biol* 1996;14:309–315.
31. Lazrak A, Nielsen VG, Matalon S. Mechanisms of increased Na(+) transport in ATII cells by cAMP: we agree to disagree and do more experiments. *Am J Physiol Lung Cell Mol Physiol* 2000;278:L233–L238.
32. Lazrak A, Samanta A, Matalon S. Biophysical properties and molecular characterization of amiloride-sensitive sodium channels in A549 cells. *Am J Physiol Lung Cell Mol Physiol* 2000;278:L848–L857.
33. Grimminger F, Weissmann N, Spriestersbach R, Becker E, Rosseau S, Seeger W. Effects of NADPH oxidase inhibitors on hypoxic vasoconstriction in buffer-perfused rabbit lungs. *Am J Physiol* 1995;268:L747–L752.
34. Goyal P, Weissmann N, Grimminger F, Hegel C, Bader L, Rose F, Fink L, Ghofrani HA, Schermuly RT, Schmidt HH, *et al.* Upregulation of NAD(P)H oxidase 1 in hypoxia activates hypoxia-inducible factor 1 via increase in reactive oxygen species. *Free Radic Biol Med* 2004; 36:1279–1288.
35. Dada LA, Chandel NS, Ridge KM, Pedemonte C, Bertorello AM, Sznajder JI. Hypoxia-induced endocytosis of Na,K-ATPase in alveolar epithelial cells is mediated by mitochondrial reactive oxygen species and PKC-zeta. *J Clin Invest* 2003;111:1057–1064.
36. Seeger W, Walmrath D, Menger M, Neuhof H. Increased lung vascular permeability after arachidonic acid and hydrostatic challenge. *J Appl Physiol* 1986;61:1781–1789.
37. Rutschman DH, Olivera W, Sznajder JI. Active transport and passive liquid movement in isolated perfused rat lungs. *J Appl Physiol* 1993;75: 1574–1580.
38. Nielsen VG, Duvall MD, Baird MS, Matalon S. cAMP activation of chloride and fluid secretion across the rabbit alveolar epithelium. *Am J Physiol* 1998;275:L1127–L1133.
39. Matthay MA, Folkesson HG, Clerici C. Lung epithelial fluid transport and the resolution of pulmonary edema. *Physiol Rev* 2002;82:569–600.
40. Sznajder JI, Factor P, Ingbar DH. Invited review: lung edema clearance: role of Na(+)-K(+)-ATPase. *J Appl Physiol* 2002;93:1860–1866.
41. Matalon S, O'Brodovich H. Sodium channels in alveolar epithelial cells: molecular characterization, biophysical properties, and physiological significance. *Annu Rev Physiol* 1999;61:627–661.
42. Kemp PJ, Kim KJ, Borok Z, Crandall ED. Re-evaluating the Na(+) conductance of adult rat alveolar type II pneumocytes: evidence for the involvement of cGMP-activated cation channels. *J Physiol* 2001; 536:693–701.
43. Elbert KJ, Schafer UF, Schafers HJ, Kim KJ, Lee VH, Lehr CM. Monolayers of human alveolar epithelial cells in primary culture for pulmonary absorption and transport studies. *Pharm Res* 1999;16:601–608.
44. Matthay MA, Ware LB. Plasma protein C levels in patients with acute lung injury: prognostic significance. *Crit Care Med* 2004;32:S229–S232.
45. Malik AB, Horgan MJ. Mechanisms of thrombin-induced lung vascular injury and edema. *Am Rev Respir Dis* 1987;136:467–470.
46. Dada LA, Sznajder JI. Mechanisms of pulmonary edema clearance during acute hypoxemic respiratory failure: role of the Na,K-ATPase. *Crit Care Med* 2003;31:S248–S252.
47. Looney MR, Sartori C, Chakraborty S, James PF, Lingrel JB, Matthay MA. Decreased expression of both the $\alpha1$ and $\alpha2$ subunits of the Na,K-ATPase reduces maximal alveolar epithelial fluid clearance. *Am J Physiol Lung Cell Mol Physiol* 2005;289:L104–L110.
48. Isenovic ER, Jacobs DB, Kedees MH, Sha Q, Milivojevic N, Kawakami K, Gick G, Sowers JR. Angiotensin II regulation of the Na+ pump involves the phosphatidylinositol-3 kinase and p42/44 mitogen-activated protein kinase signaling pathways in vascular smooth muscle cells. *Endocrinology* 2004;145:1151–1160.

49. Sasson R, Dantes A, Tajima K, Amsterdam A. Novel genes modulated by FSH in normal and immortalized FSH-responsive cells: new insights into the mechanism of FSH action. *FASEB J* 2003;17:1256–1266.
50. Lecuona E, Garcia A, Sznajder JI. A novel role for protein phosphatase 2A in the dopaminergic regulation of Na,K-ATPase. *FEBS Lett* 2000; 481:217–220.
51. Ridge KM, Dada L, Lecuona E, Bertorello AM, Katz AI, Mochly-Rosen D, Sznajder JI. Dopamine-induced exocytosis of Na,K-ATPase is dependent on activation of protein kinase C-epsilon and -delta. *Mol Biol Cell* 2002;13:1381–1389.
52. Lei J, Mariash CN, Ingbar DH. 3,3′,5-Triiodo-L-thyronine up-regulation of Na,K-ATPase activity and cell surface expression in alveolar epithelial cells is Src kinase- and phosphoinositide 3-kinase-dependent. *J Biol Chem* 2004;279:47589–47600.
53. Cooper JA. Effects of cytochalasin and phalloidin on actin. *J Cell Biol* 1987;105:1473–1478.
54. Dada LA, Santos BF, Lecuona E, Sznajder JI. The actin cytoskeleton is required for hypoxia-mediated Na,K-ATPase endocytosis in alveolar epithelial cells [abstract]. *Am J Respir Crit Care Med* 2004;160:A412.
55. Gorlach A, Brandes RP, Nguyen K, Amidi M, Dehghani F, Busse R. A gp91phox containing NADPH oxidase selectively expressed in endothelial cells is a major source of oxygen radical generation in the arterial wall. *Circ Res* 2000;87:26–32.
56. Li X, Hahn CN, Parsons M, Drew J, Vadas MA, Gamble JR. Role of protein kinase Czeta in thrombin-induced endothelial permeability changes: inhibition by angiopoietin-1. *Blood* 2004;104:1716–1724.
57. Li Y, Trush MA. Diphenyleneiodonium, an NAD(P)H oxidase inhibitor, also potently inhibits mitochondrial reactive oxygen species production. *Biochem Biophys Res Commun* 1998;253:295–299.
58. Ragan CI. The molecular organization of NADH dehydrogenase. *Subcell Biochem* 1980;7:267–307.
59. Konishi H, Tanaka M, Takemura Y, Matsuzaki H, Ono Y, Kikkawa U, Nishizuka Y. Activation of protein kinase C by tyrosine phosphorylation in response to H_2O_2. *Proc Natl Acad Sci USA* 1997;94:11233–11237.
60. Chibalin AV, Pedemonte CH, Katz AI, Feraille E, Berggren PO, Bertorello AM. Phosphorylation of the catalyic alpha-subunit constitutes a triggering signal for Na+,K+-ATPase endocytosis. *J Biol Chem* 1998;273:8814–8819.
61. Feschenko MS, Sweadner KJ. Phosphorylation of Na,K-ATPase by protein kinase C at Ser18 occurs in intact cells but does not result in direct inhibition of ATP hydrolysis. *J Biol Chem* 1997;272:17726–17733.
62. Bachofen H, Schurch S, Weibel ER. Experimental hydrostatic pulmonary edema in rabbit lungs. Barrier lesions. *Am Rev Respir Dis* 1993;147: 997–1004.
63. Cottrell TS, Levine OR, Senior RM, Wiener J, Spiro D, Fishman AP. Electron microscopic alterations at the alveolar level in pulmonary edema. *Circ Res* 1967;21:783–797.
64. Bhattacharya J, Gropper MA, Staub NC. Interstitial fluid pressure gradient measured by micropuncture in excised dog lung. *J Appl Physiol* 1984;56:271–277.
65. Bhattacharya J. The alveolar water gate. *Am J Physiol Lung Cell Mol Physiol* 2004;286:L257–L258.